Effect of TiO2 on morphology and mechanical properties of PVDF/PMMA blend films prepared by melt casting process

Title:

Effect of TiO_2 on morphology and mechanical properties of PVDF/PMMA blend films prepared by melt casting process

Authors:

Tomonori Hosoda*
Polymer Processing Technology Center, Kureha Corporation
Omitama-city, Ibaraki 311-3436, Japan
Division of Material Science, Kanazawa University,
Kakuma-machi, Kanazawa, 920-1192, Japan
Tel; +81-299-26-7942
FAX; +81-299-26-7943

Toshiro Yamada
Division of Material Science, Kanazawa University,
Kakuma-machi, 920-1192, Japan

*To whom all correspondence should be addressed.
Email; t-hosoda@kureha.co.jp

Abstract

Effect of titanium dioxide (TiO_2) on morphology and mechanical properties of poly(vinylidene fluoride) (PVDF)/poly(methyl methacrylate) (PMMA) blend films prepared at different TiO_2 contents by a melt casting process was studied. The results showed that tensile moduli in both the machine direction (MD) and the transverse direction (TD) increased with increasing TiO_2 content, and calculated tensile moduli based on the Halpin-Tsai and the Kerner model were consistent with experimental ones in both the MD and TD of films containing 10 wt% TiO_2. However, experimental tensile moduli exhibited smaller values compared with calculated ones, as the TiO_2 content increased to 30 wt%, and it was assumed that this is due to the decrease of crystallinity of PVDF. Morphological observations indicated that TiO_2 particles did not affect crystal structures of PVDF and the morphology of PVDF/PMMA amorphous phase, but hindered the crystallization of PVDF. The MD and TD elongation at break exhibited >200% and <20%, respectively. The SEM micrographs revealed that spherulites could deform along the MD when the tensile force was applied along the direction. By contrast, spherulites could not deform along the TD and fractured at very small elongation, owing to the anisotropic morphology of spherulites.

Introduction

Poly(vinylidene fluoride) (PVDF) is a semicrystalline polymer that is widely used in industry because of its excellent mechanical properties, good chemical resistance to severe environmental stress [1, 2]. However, PVDF has week adhesion to other polymers due to low surface tension resulted from its molecular structure. In order to improve adhesive properties of PVDF, many kinds of polymer blends were studied with respect to interaction between fluorine atoms in PVDF and carbonyl groups in a partner polymer [3–5]. According to those researches, the improvement of adhesive properties is not expected when PVDF forms matrix phase. On the other hand, excellent properties such as chemical resistance and long-term weatherability lose when PVDF forms domain phase in composite materials. In the early 1960's, it was discovered that PVDF and poly(methyl methacrylate) (PMMA) are molecularly miscible in the amorphous state, and the blend material has been studied extensively up to the present time, because the blend materials gave economic efficiency and good mechanical properties [6–8].

There are several reports on the polymer blends of PVDF and PMMA. The general conclusion is that such systems exhibit lower critical solution temperature (LCST) behavior around 330°C. Therefore, these components are miscible in the amorphous state above the melting point of PVDF (Tm ≅ 170°C), and PVDF crystallizes from the melt state below the Tm if the blend is maintained above its glass transition temperature (Tg) [9–16].

It is well known that PVDF can crystallize into at least four different crystal structures (α, β, γ, and δ) [17]. Crystal structures of PVDF depended on crystallization temperatures during melting process and stretching conditions [18-24]. For PVDF/PMMA blend materials, crystal structures were dominated by cooling conditions and the blend ratio of PVDF/PMMA [25, 26].

In the aim of the improvement of outstanding properties for PVDF films, titanium dioxide (TiO_2), one of the inorganic materials, has received the most attention because of its excellent properties such as long-term stability, nontoxicity, and resistance to discoloration under UV light. Cao et al. reported that the small nanoparticles (average diameter: ~10 nm) improved the antifouling property of the PVDF membranes and had a substantial effect on the crystallization of PVDF [27]. In addition, the crystallinity of PVDF decreased, as the ratio of TiO_2 nanoparticle (average diameter of ~400 nm) in the PVDF increased [28].

Economic efficiency, an improvement of adhesive properties to other materials, and hydrophilicity are expected by adding PMMA to PVDF. Since TiO_2 particles have superior properties as mentioned above, there are

several reports on PVDF/PMMA/TiO_2 composite materials. Zhao et al. prepared PVDF/PMMA/TiO_2 composite materials by adding TiO_2 nanoparticles (1–5 wt%) during the in situ polymerization of methyl methacrylate (MMA) in PDVF. They revealed that the hydrophilicity was enhanced as the TiO_2 content increased [29]. For PVDF/PMMA/TiO_2 (65/20/15, wt/wt/wt) blend films prepared by the melt casting process, crystal structures of PVDF were studied. The result showed that the β phase of PVDF was formed and its structural conversion to the α phase was observed with increasing chill roll temperature [30]. In addition, for PVDF/PMMA/TiO_2 (80/20/30, wt/wt/wt) blend films, the α phase of the PVDF was formed when the chill roll temperature was above 78°C. Based on the morphological study, it was suggested that the excluded PMMA was entrapped within the interlamellar region in the spherulites because of the fast growth rate of the α phase [31]. Tang et al. studied melt-mixed PVDF, PVDF/PMMA and PVDF/PMMA/TiO_2 blown films developed for solar cell encapsulation. In the study, they found that PVDF films formed the α phase, and PVDF/PMMA films containing 10, 20, and 30 wt% PMMA exhibited coexistence of the α and β phase.

With regard to mechanical properties, the addition of 15 wt% TiO_2 to PVDF/PMMA blends (70/30, wt/wt) improved the elongation at break of the blown film compared with the film which were not containing TiO_2 [32]. In a different study of PVDF/PMMA/TiO_2 blend films, it was reported that the addition of 2–10 wt% TiO_2 (primary diameter of 260–300 nm) to PVDF/PMMA (70/30, wt/wt) resulted in an improvement in the tensile strength and elongation at break [30]. Lee et al. found that the elongation at break increased in the value from 0 to 10 wt% TiO_2 in the composite, followed by a decrease beyond 10 wt% [33]. Those results showed that PVDF/PMMA/TiO_2 blend films exhibited good mechanical properties. In addition, PVDF/PMMA/TiO_2 blend films are a promising material for a photovoltaic cell and module because of long-term weatherability. One of the studies revealed that the weatherability of the β phase of PVDF in the film after pressure cooker test (PCT) decreased as a result of yellowing because of the unstable structure of β phase [33–34].

Our previous study showed the crystalline orientation in PVDF/PMMA/TiO_2 blend films prepared by a melt casting process with a slit die, which is one of the melt casting process [31]. However, there is no investigation how orientation of crystals influences mechanical properties, although anisotropic morphology is an important factor dominating film properties in practical use. In addition, there are few reports on the effect of TiO_2 with regards to morphology and mechanical properties of PVDF/PMMA

blend films. Lee et al. reported mechanical properties with respect to different TiO_2 contents on PVDF/PMMA/TiO_2 blend films cast at the chill roll temperature of 50°C, and they did not mention the blend ratio of PVDF/PMMA and anisotropic morphology on the film [34].

Therefore, we focused to study the effects of TiO_2 on mechanical properties and morphology of PVDF/PMMA blend films prepared by a melt casting process in terms of machine direction (MD) and transverse direction (TD). The morphology of PVDF/PMMA and PVDF/PMMA/TiO_2 blend films was evaluated by using wide-angle X-ray diffraction (WAXD), scanning electron microscopy (SEM), and dynamic mechanical analysis (DMA). Mechanical properties were conducted by a using tensile tester.

Experimental

Materials

The PVDF used in this study was supplied by Kureha Corporation (Japan), and the molecular weights were 194,000 (Mw) and 86,000 (Mn). The PMMA was purchased from Asahi Kasei Chemicals (Japan), and the molecular weights measured by gel-permeation chromatography were 130,000 (Mw) and 86,000 (Mn). The rutile TiO_2 particles (average diameter: ~290 nm) was purchased from DuPont (Wilmington, DE, USA).

Film preparation

PVDF/PMMA/TiO_2 blend films were prepared by a melt casting process with a slit die. The composition of PVDF/PMMA was fixed at the weight ratio of 80:20. 0, 10, 20, 30 wt% TiO_2 particles were added to the PVDF/PMMA blend materials. The composite materials of PVDF/PMMA/TiO_2 were first pelletized by using a twin screw extruder. After obtaining pellets, films (20 μm in thickness) were extruded and cast at the chill roll temperature of 100°C. The barrel temperature was 240°C, the width of the slit die was 270 mm, and the die gap was 0.5 mm. The shear rate was calculated to be 38 sec^{-1} from the extrusion output of 3.1 kg/h, density of 1.7 g/cm^3 of the PVDF/PMMA blend material, and die size. Different TiO_2 contents of 0, 10, 20, and 30 wt% in PVDF/PMMA (80/20, wt/wt) blend materials were applied in this study. The corresponding films were coded as PMTi-0, PMTi-10, PMTi-20 and PMTi-30, respectively.

Measurements

The film surface temperature during the melt casting process was measured

by a contact thermometer. The measured area was not evaluated in this study because its appearance was insufficient. In this study, chill roll temperature refers to the surface temperature of the chill roll measured by the contact thermometer.

Tensile modulus was measured with an Tensilon RTM-100(Toyo Baldwin Co., Japan) at 23°C and 50% humidity. The specimen size was 20 mm wide by 100 mm long (gauge length), and the crosshead speed was 10 mm/min. Elongation at break was performed by the equipment and environment. The specimen size was 10 mm wide by 50 mm long with 500 mm/min in the crosshead speed. In order to measure Poisson's ratio, strain is measured both in the tensile direction and at horizontal direction using an Autograph (model AG-kNXPlus, Shimazu Seisakujyo Co., Japan) and a noncontact displacement gauge (model, TRViewX500D, Shimazu Seisakujyo). The original distance between gauge marks of length and wide was 25 mm and 10 mm respectively. The crosshead speed was 5 mm/min at 23°C.

WAXD measurements were performed using a NANO-Viewer system (Rigaku Co., Japan). Cu–Kα radiation (40 kV, 20 mA) was generated and collimated by a confocal mirror system. The wavelength and the camera length were 1.54 Å and 70 mm, respectively. An imaging plate (IP), (BAS-SR 127, Fujifilm Co., Japan) was used as a two-dimensional detector, and the IP reading device RAXIA-Di (Rigaku Co.) was employed to transform the obtained image into text data.

The cross sections of PVDF/PMMA/TiO_2 films were prepared using an ion milling system (model IM4000, Hitachi Hightechnologies Co., Japan) with 4 kV for 1 h in cold atmosphere with liquid nitrogen. The samples were observed using SEM (model 8020, Hitachi Hightechnologies) with the accelerating voltage of 1 kV.

The morphology of the film surfaces was observed using the SEM with the accelerating voltage of 3 kV after coating platinum particles under vacuum-dried conditions.

DMA measurements were conducted by using an RSA-3 device (TA Instruments Inc., USA) at the heating rate of 2°C/min. The frequency was 10 Hz and the temperature range was from −80°C to 120°C.

Results and Discussion

Film temperature during the melt casting process

Figure 1 shows the film temperature profile of PVDF/PMMA blend films during the melt casting process at the chill roll temperature of 100°C. Zero

seconds on the x axis refers to the time at which the molten material just begins to flow from the die gap. As seen the figure, a rapid decrease in the film temperature begins at 2.6 s because the molten material contacted the chill roll at this time. It was found that the film temperature reached 102°C at 4.2 s. The film was pealed from the chill roll after casting for 10 s. The film was wound at room temperature after pealed the chill roll. This result indicates that the cooling system is sufficient for allowing the films to reach the chill roll temperature.

Effect of TiO_2 on tensile modulus and morphology

Figure 2 shows tensile moduli in the MD and the TD of films as a function of TiO_2 content. MD is parallel with the material flow during the melt casting process. TD is known as the cross direction to MD. Tensile moduli of PMTi-0 are approximately 2300 MPa in both the MD and the TD. The tensile moduli increased with increasing TiO_2 content, and that of PMTi-30 reached approximately 3000 Mpa in both the MD and the TD. The tensile modulus in the MD showed slightly higher than that in the TD, regardless of the TiO_2 content for all samples. Our previous study on PVDF/PMMA/TiO_2 (80/20/30, wt/wt/wt) blend films observed that molecular chains of PVDF had the slight MD orientation in films prepared by the melt casting process with the slit die when the chill roll temperature was above 90°C [31]. We confirmed the MD orientation of PVDF crystals for all samples by WAXD measurements in this experiment. Therefore, it is assumed the reason of the slightly higher modulus in the MD compared with that in the TD is the orientational effect.

In general, incorporating inorganic nanoparticles into polymer matrix is a practical way to obtain advanced materials of composites [35]. It is well known that tensile modulus of a two-phase blends depends on the size, shape, and distribution of dispersed particles or the coarseness and tortuosity of a continuous phase. Several theories were developed to predict the modulus of a two-phase blends [36–41]. It is estimated that PVDF/PMMA composite materials form matrix phase and TiO_2 particles disperse in the matrix. Therefore, it is expected that tensile modulus of films should be predicted by the theories which are the parallel model [36–39], the series model [36–39], the Halpin–Tsai model, and the Kerner model [37, 39]. Using these models, we examined dispersed state of TiO_2 particles and morphology of the matrix.

Parallel model is given by Equation (1), and represents the upper bounds of the tensile modulus. This model is applicable to materials in which the components are connected parallel to one another so that the applied stress lengthens each component to the same extent.

$$E = E_1\varphi_1 + E_2\varphi_2$$

(1)

Series model represents the lower bounds of the tensile modulus, and given by Equation (2). For the model, the blend components are arranged series perpendicular to the direction of the applied force.

$$\frac{1}{E} = \frac{\varphi_1}{E_1} + \frac{\varphi_2}{E_2} \tag{2}$$

where E is the tensile modulus of the blend material. E_1 and E_2 are tensile moduli of components 1 and 2. φ_1 and φ_2 are corresponding to volume fractions of components 1 and 2 [36, 37].

Halpin–Tsai model given by Equation (3) has been successfully applied by several researchers to systems of binary polymer composites [36, 37].

$$\frac{E_1}{E} = \frac{(1 + A_i B_i \varphi_2)}{(1 - B_i \varphi_2)} \tag{3}$$

where

$$B_i = \frac{(E_1/E_2) - 1}{(E_1/E_2) + A_i} \tag{4}$$

In the Halpin–Tsai Equation, subscripts 1 and 2 refer to the continuous and dispersed phases, respectively. The constant A_i is defined by morphology of the system. For elastomer domains dispersing in a continuous hard matrix, A_i is 0.66. Instead, if the hard material forms the dispersed phase, A_i is 1.5 [37, 38].

Another important model for perfect adhesion between a continuous and dispersed phase is the Kerner Equation. Kerner derived a theory for a matrix with spherical inclusions, when the system is isotropic and adhesion between the two phases is perfect. The Kerner model is given by equation (5) [37, 39].

$$E = E_m \left[\frac{\varphi_d E_d/[(7 - 5\upsilon_m)E_m + (8 - 10\upsilon_m)E_d] + \varphi_m/15(1 - \upsilon_m)}{\varphi_d E_m/[(7 - 5\upsilon_m)E_m + (8 - 10\upsilon_m)E_d] + \varphi_m/15(1 - \upsilon_m)} \right. \tag{5}$$

where E is the tensile modulus of the blend material, υ is Poisson's ratio of the matrix, and φ is the volume fraction. The subscripts m and d stand for the matrix and dispersed phase, respectively. Those models are applicable to a two-phase systems and useful for the prediction of the phase morphology in

the system that TiO_2 particles disperse in PVDF/PMMA matrix. Figure 3 shows the SEM micrographs of the cross section of PMTi-30. As seen in Figure 3, the dispersity of TiO_2 was mostly homogeneous in the polymer matrix. We also confirmed that the dispersity of TiO_2 particles was improved as the TiO_2 content decreased in the composites.

Figure 4 shows comparisons of the calculated and the experimental curves of the tensile modulus in the MD as a function of TiO_2 content. Figure 5 represents those in the TD. For comparison, experimental tensile moduli exhibited in Figure 2 are also shown in Figure 4 and 5. Experimental tensile moduli in the MD and TD of PVDF/PMMA blend films with 0 wt% TiO_2 were adopted as the value of a continuous phase, when calculating tensile moduli of PMTi-10, PMTi-20, and PMTi-30. In addition, the tensile modulus of 283 GPa was used for the calculation as the value of TiO_2 particle [40]. Since TiO_2 is a harder material than the matrix, 1.5 of A_i is used for the Halpin–Tsai Equation. For the calculation of the Kerner model, the experimental values of the Poisson's ratio (MD: 0.040, TD: 0.042) was adopted.

As seen in Figure 4 and 5, moduli calculated by the series model exhibited smaller values compared with experimental moduli for all samples. By contrast, calculated moduli obtained from the parallel model attained extremely higher values. The moduli of PMTi-0 calculated by parallel model were approximately 14000 Mpa in the MD and TD. On the other hand, moduli of PMTi-10 calculated by the Halpin–Tsai model and the Kerner model were consistent with experimental moduli in the MD and TD. From these results, the isotropic dispersity of TiO_2 particles was indicated. Furthermore, it was estimated that the adhesion between TiO_2 particles and the PVDF/PMMA phase is significantly stronger under the strain in tensile measurements, which is less than 1%. However, experimental moduli of PMTi-20 and PMTi-30 in both the MD and TD were smaller values compared with calculated ones obtained from the Halpin–Tsai and Kerner model.

Figure 6 represents the WAXD profiles with different TiO_2 contents. All samples showed similar WAXD profiles, regardless of the TiO_2 content. All profiles had peaks 2θ of 17.4°, 18.2°, and 19.8°, and these peaks correspond to the α phase Bragg diffraction of (100), (020), and (110), respectively [30, 31, 33]. As seen in the Figure, all samples prepared at the chill roll temperature of 100°C formed the α phase of PVDF. Therefore, it was revealed that TiO_2 particles had no significant effect on crystal structures of PVDF. Based on the WAXD profiles, crystallinity was calculated by Equation (6).

$$Xc\ (\%) = \frac{A_c}{A_\alpha + A_c} \times 100$$

where Ac is the area of the crystalline phase and Aα is the area of the amorphous in the WAXD profiles presented in Figure 6. Figure 7 shows crystallinity with different TiO_2 contents. The crystallinity of either PMTi-0 or PMTi-10 was 35%. However, the crystallinity followed by a decrease beyond 10 wt% TiO_2, and the crystallinity of PMTi-20 and PMTi-30 was 32% and 25%, respectively. As mentioned above, calculated tensile moduli were obtained by using experimental tensile moduli in the MD and TD of the PVDF/PMMA blend film which does not contain TiO_2 particles, so that it is assumed the deviation to lower side of experimental tensile moduli for films containing 20−30 wt% TiO_2 is due to the decrease of the crystallinity. If the modulus of PMTi-20 and PMTi-30 by the crystallization decreases approximately 4% and 7%, respectively, the experimental tensile modulus mostly coincided with calculated one obtained from the Halpin-Tsai model.

Figure 8 shows the SEM micrographs of the film surfaces of both chill roll side and the opposite one of PMTi-0 and PMTi-30. There are no significant difference between the chill roll side and the opposite one. Sheaflike spherulites can be clearly seen in PMTi-0, and both sheaflike spherulites and TiO_2 particles can be clearly seen in PMTi-30. Generally, inorganic particles act as a nucleus and enhance crystallinity [41, 42], and it was reported that the increase of crystallization temperature in the cooling process were observed in PVDF/PMMA/TiO_2 blend materials by differential scanning calorimetry (DSC). This result indicates that TiO_2 particle acts as a nucleus regent [33, 34]. However, on carefully study of the SEM micrographs of PMTi-30, it seems that TiO_2 particles hinder the crystal growth owing to the existence of TiO_2 particles. This observation is clearly recognized within the dotted circles in the micrographs. From the morphological observations, it was found that the decrease of crystallinity with increasing TiO_2 content was due to hindrance of crystal growth by some of TiO_2 particles, even though different TiO_2 particles acted as a nucleus regent. In addition, the MD orientation of PVDF chains is recognized because most of lamellae in sheaflike spherulites grow along the TD, as seen in all SEM micrographs.

Figure 9 and 10 shows plots of the storage modulus (E') versus temperature in the TD of films. Figure 10 denotes plots of the loss modulus (E") versus temperature in the TD of films. With increasing TiO_2 content, the values of E' increased over the entire temperature range. This was similar result to the tensile modulus shown in Figure 2. All samples exhibited peaks of the E" curves at approximately -45°C and 55°C, as seen in Figure 10. Hirata et al. clearly defined the E" peaks for PVDF/PMMA composite

materials obtained by melt-mixed blends [43, 44]. According to their reports, there is a four-phase morphology in the melt mixed PVDF/PMMA blend materials that the PVDF content is >60 wt%. The four-phase morphology composed of a mixed amorphous phase with Tg≈55°C, an amorphous PVDF phase with Tg≈-40°C, an imperfect crystalline phase, and a nearly pure PVDF crystalline phase [43, 44]. PVDF/PMM/TiO_2 blend films prepared at various chill roll temperatures from 30°C to 115°C by the melt casting process with the slit die exhibited peaks at the similar temperature [33]. Therefore, based on previous studies, the peak observed near 55°C is attributed to the mixed amorphous phase, and that near -45°C is attributed to the amorphous PVDF phase for the films. It was found that the peak positions ascribed to the mixed amorphous phase of PVDF/PMMA was not affected by adding TiO_2 particles in our experiments. We also confirmed that peaks in the E" curves seen in the MD of films was the similar results.

Based on the theories on the tensile modulus for binary blends and the SEM micrographs, it was revealed that TiO_2 particles in the PVDF/PMMA/TiO_2 blend films disperse homogeneously in the polymer matrix and the system is isotropy and significant adhesion between the two phases. It was suggested that TiO_2 particles used in the experiment did not affected both the crystal structure of PVDF and the morphology of PVDF/PMMA mixed amorphous, but hindered the crystallization of PVDF.

Anisotropy on elongation at break of films

Figure 11 shows the effect of TiO_2 content on the MD and the TD elongation at break of films. The MD elongation at break of PMTi-0 represents 230%, and that of PMTi-10 reached 330%. This increment is because TiO_2 particles functioned as physical junctions in the film during the extrusion [34]. Beyond 10 wt% TiO_2 content, the elongation at break decreased with increasing TiO_2 content in the film, and the MD elongation at break of PMTi-30 became 280%. Meanwhile, the TD elongation at break of PMTi-0 was 9%, and the value was quite small compared with that of 230% seen in the MD elongation at break of PMTi-0. The TD elongation at break slightly increased with increasing TiO_2 content, and that of PMTi-30 reached 21%. The results mean that films have an extreme anisotropy property with regard to elongation at break. In order to investigate the cause resulting in the anisotropic properties, we examined the relationship between spherulitic morphology and stress–strain (S–S) behavior.

Figure 12 shows the S–S curves and the SEM micrographs of the film surfaces when tensile force was applied along the MD. Figure 13 shows that in the TD. The SEM micrographs of the film surfaces seen in Figure 12

correspond to 200% and 170% elongation of PMTi-0 and PMTi-30, respectively. When comparing the SEM image of the film surfaces between 0% elongation seen in Figure 8 and 200% elongation seen in Figure 12, it was found that spherulites deformed significantly along the MD. For PMTi-30, it was observed not only the deformation of spherulites but also the interfacial peeling (shown within the dotted circles) between TiO_2 particles and the matrix. It was thought that the interfacial peeling is the reason for the decrease of the elongation with increasing TiO_2 content beyond 10 wt%. It was also reported in a different paper that the elongation at break decreased beyond 10 wt% along with the reduction of crystallinity, because lower crystallinity would break at a smaller stress [33].

On the other hand, the morphological observation for the TD seen in Figure 13 identified that cracks perpendicular to direction of the applied force were seen within spherulites. This event was observed regardless of incorporation of TiO_2 particles. PVDF crystals in films used in this experiment have the MD orientation, and the fact can be judged from our previous study [31] and the growth direction of lamellar seen in Figure 8 as mentioned above.

For PVDF/PMMA blend materials, PVDF crystalized with the exclusion of PMMA and the excluded PMMA existed in the amorphous pockets [8, 45] Therefore, when tensile force was applied along MD of the film, it is expected that spherulites deform easily under stress because the flexible amorphous existing within the interlamellar region can be stretched along the applied force. By contrast, when tensile force is applied along TD, lamellae themselves are compelled to the deformation of spherulites. Thus, the reason why films fractured at the small elongation because the spherulites could not endure the stress. Based on the morphological observations, it was deduced that the remarkable anisotropy on the elongation at break of films is due to the orientation of PVDF crystals, and the orientation is owing to the flow field caused by the melt casting process with the slit die. Figure 14 shows a schematic illustration when tensile force was applied along MD and TD. Furthermore, the yield stress of PMTi-0 was higher than that of PMTi-30 for either the MD or the TD, as seen in Figure 12 and 13. This probably resulted in higher crystallinity of PMTi-0 because yield stress is attributed to tilting stress for lamellae in spherulites.

Conclusion

PVDF/PMMA/TiO_2 blend films were prepared by a melt casting process, and effect of TiO_2 on morphology and mechanical properties was studied using WAXD, SEM, DMA, and tensile testing machine. As increasing TiO_2 content, tensile moduli in both the MD and TD increased, and the modulus in the MD had slightly higher value than that in the TD regardless of the TiO_2 content. This is due to the MD orientation of PVDF crystals. Prediction of the tensile modulus by using several theories was conducted. As a result, tensile moduli calculated by the Halpin-Tsai and the Kerner model were consistent with experimental moduli in both the MD and TD for PVDF/PMMA blend films containing 10 wt% TiO_2. However, experimental tensile moduli exhibited smaller values compared with calculated ones, as the TiO_2 content increased to 30 wt%. Based on morphological observations, it was revealed that TiO_2 particles did not affect the crystal structures of PVDF and the morphology of the PVDF/PMMA amorphous phase, but hindered the crystallization. From the results, it was deduced that the deviation between the calculated and the experimental tensile modulus was due to the decrease of crystallinity.

In the study on the elongation at break of films, the MD elongation at break represented more than 200%, and the TD elongation at break exhibited less than 20%. Based on the result of the S-S behavior and the SEM micrographs of the film surfaces, it was identified that sheaflike spherulites can deform along the MD when tensile force is applied along MD of the film. The reason why such spherulites can deform along the MD is due to stretching of the amorphous phase existing within the interlamellar region. By contrast, sheaflike spherulites fractured when tensile force applied along TD, because lamellae themselves were compelled to deformation and could not deform along the TD, because of the orientation of PVDF crystals. Therefore, it was deduced that such properties of elongation at break is caused by the anisotropy of spherulites formed owing to the flow field caused by the melt casting process with the slit die.

Acknowledgement

The authors acknowledge helpful discussion and cooperation in performing these experiments with Tetsuya Komatsuzaki (Kureha Extech Co., Ltd), Tomoyuki Hidaka (Kureha Corporation), Kazuyuki Suzuki (Kureha Corporation) during 2012–2013. SEM observations were carried out by Sanae Kamata (Kureha Corporation).

References

[1] McCarthy, RA, *Encyclopedia of Polymer Science and Engineering*, Vol, 3, ed., John Wiley, New York, 1985.
[2] Scheinbeim JI, *Polymer Data Handbook*, Oxford Univ. Press, Oxford, UK. 1999
[3] Lee WK, Ha CS. *Polymer* 1998, 39, 7131-7134
[4] Salim A. Yousefi AA. *J. Polym. Sci.* 2004, B42, 3487-3495
[5] Huang C. Zhang L. *J. Appl. Polym. Sci.* 2004, 92, 1-5
[6] Hourston DJ, Hughes ID. *Polymer* 1977, 18, 1175-1178
[7] Wendorff H, Ullmann W. *Comp. Sci. and Tech*. 1985, 23, 97-112
[8] Cebe P, Chung SY. *J. Mater. Sci*. 1990, 25, 2367-2378
[9] Bernstein RE, Barlow JW. Macromolecules 1977, 10, 3, 681
[10] Noland JS, Schmitt JM. *Adv. Chem. Ser.*, 1971, 99, 15
[11] Nishi T, Wang TT. *Macromolecules* 1975, 8, 909
[12] Wang, TT, Nishi T. *Macromolecules* 1977, 10, 421
[13] Douglass D, McBrierty VJ. *Macromolecules* 1978, 11, 766
[14] Chuang H, Han CD. *J. Appl. Polym. Sci*. 1984, 29, 2205
[15] Wolf M, Wendorff JH. *Polymer* 1989, 30, 1524
[16] Yang H, Han CD. *Polymer* 1994, 35, 1503
[17] Tashiro K, *Ferroelectrics* 1981, 32, 167
[18] Nakamura S, Sasaki T. *Makromol Chem*. 1975, 176, 3471
[19] Welch GJ, Miller RL. *J. Polym. Sci. Polym. Phys. Ed*. 1976, 14, 1683
[20] Mancaella L. *Polymer* 1977, 18, 1240
[21] Prest MW. Jr, Luca DJ. J Appl. Phys. 1979, 46, 4136
[22] Lonvinger AJ, Keith HD., *Macromolecules* 1979, 12, 919
[23] Morra BS, Stein RS. *J. Polym. Sci. Polym*. Phys. Ed. 1982, 11, 2243
[24] Hsu TC, Geil PH. *J. Mater. Sci*. 1989, 24, 1219
[25] Horibe H, Baba F. *Nippon Kagaku Kaishi* 2000, No.2, 121
[26] Horibe H, Taniyama M. *J. Electrochem. Soc*. 2006, 153, G119

[27] Cao X, Ma J. *Applied Surface Sci*. 2006, 253, 2003-2010
[28] Rekik H, Boiteux G, Kallel A. *Composites* Part B, 2013, 45, 1199-1206
[29] Zhao X, Wang X. *J. Polym. Res*. 2012, 19, 9862-9871
[30] Lee JG, Kim SH. *Macro. Res*. 2011, 19, 72-78
[31] Hosoda T, Yamada T. *J. Polym. Eng*. 2013, 33, 639-649
[32] Tang E, Yuan H. *J. Mater. Sci*. 2011, 46, 6656-6663
[33] Lee JG, Park SH. *Macro. Res*. 2013, 21, 349-355
[34] Li W, Li H. *J. Mater. Sci.* 2009, 44, 2977-2984
[35] Long Y, Shanks RA. *J. Appl. Polym. Sci*. 1996, 61, 1877-1885
[36] Gregor-Svetec D. *J. Appl. Polym. Sci*. 2000, 75, 1211-1220
[37] Joseph S, Thomas S. *J. Polym. Sci. Part B*, 2002, 40, 755-764
[38] Senuma A, *Nippon Gomu Kyokaishi* 2003, 76, 86-89
[39] Robeson LM, Merriam CN. *Macromolekulare Chemine* 1973, 29/30, 47-62
[40] Shackelford JF, Alexander W. Materials Science and Engineering Handbook, CRC Press, New York, 2001
[41] Feng Y, Hay JN. *J Applied Polym. Sci.* 1998, 69, 2089-2095
[42] Huang Y, Wu Y. *European Polymer Journal* 2005, 41, 2753-2760
[43] Hirata Y, Kotaka T. *Reports on Progress in Polymer Physics in Japan*, 1979, XXⅡ, 177-180
[44] Hirata Y, Kotaka T. *Polymer J.* 1981, 13, 3, 273-281
[45] Okabe Y, Saito H. *Polymer*, 2010, 51, 1494-1500

Captions

Figure 1. The film temperature profile during the melt casting process. (Chill roll temperature; 100°C)

Figure 2. Tensile modulus of PVDF/PMMA/TiO_2 blend films with different TiO_2 contents.

Figure 3. SEM micrograph of the cross section of PMTi-30.

Figure 4. Comparison of the experimental tensile modulus and theoretical prediction in machine direction (MD) for PVDF/PMMA/TiO_2 blend films.

Figure 5. Comparison of the experimental tensile modulus and theoretical prediction in transverse direction (TD) for PVDF/PMMA/TiO_2 blend films.

Figure 6. WAXD profiles of PVDF/PMMA/TiO_2 blend films with different TiO_2 contents.

Figure 7. Crystallinity of PVDF/PMMA/TiO_2 blend films with different TiO_2 contents.

Figure 8. SEM micrographs of film surfaces: (A) chill roll side for PMTi-0, (B) opposite side of chill roll for PMTi-0, (C) chill roll side for PMTi-30, (D) opposite side of chill roll for PMTi-30.

Figure 9. Temperature dependence of storage modulus, E′, for PVDF/PMMA/TiO_2 blend films with different TiO_2 contents.

Figure 10. Temperature dependence of loss modulus, E″, for PVDF/PMMA/TiO_2 blend films with different TiO_2 contents.

Figure 11. Elongation at break of PVDF/PMMA/TiO_2 blend films with different TiO_2 contents.

Figure 12. Engineering stress–strain curves for PMTi-0 and PMTi–30 in MD, and SEM micrographs of film surfaces: (A) 200% elongation of PMTi-0, (B) 170% elongation of PMTi-30

Figure 13. Engineering stress–strain curves for PMTi-0 and PMTi-30 in TD, and SEM micrographs of film surfaces: (A) 4% elongation of PMTi-0, (B) 8% elongation of PMTi-0, (C) 20% elongation of PMTi-30.

Figure 14. Schematic illustration at deformation of spherulites.

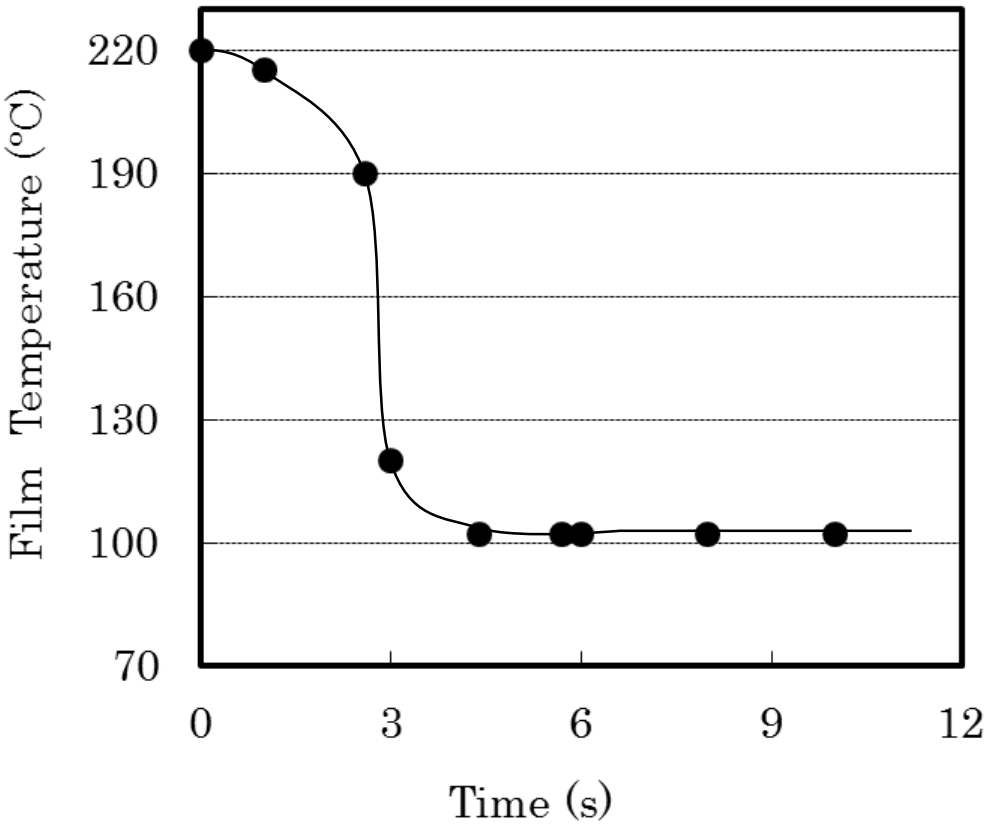

Fig. 1

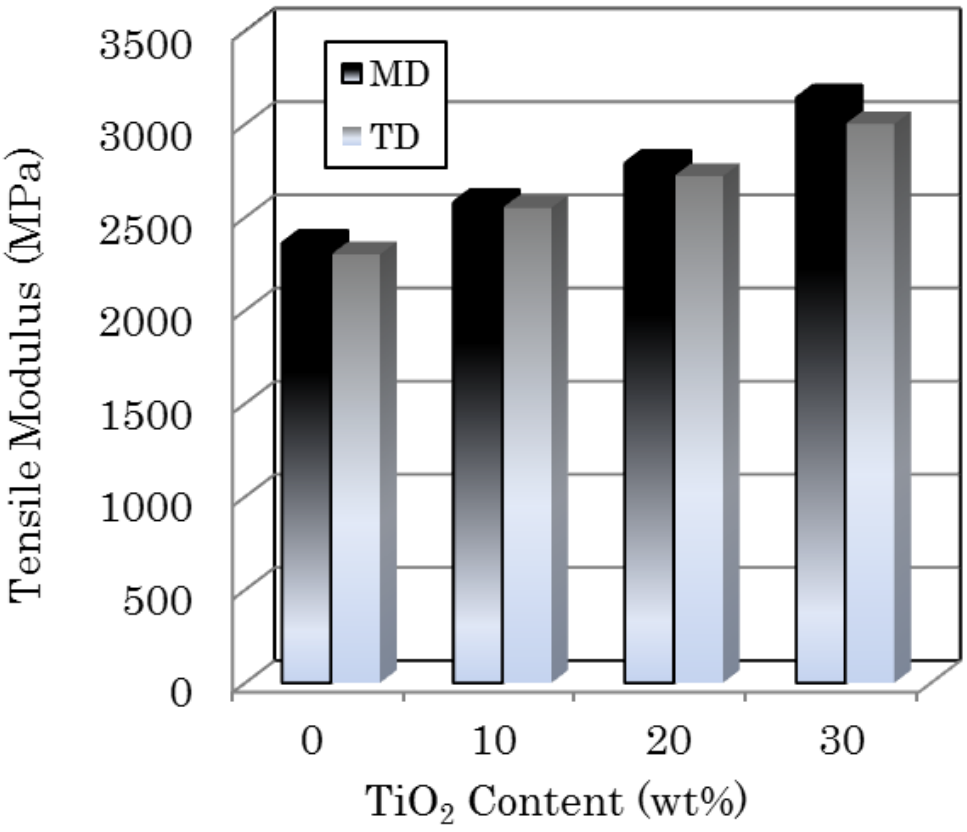
Tensile Modulus (MPa)
3500
3000
2500
2000
1500
1000
500
0
MD
TD
0
10
20
30
TiO2 Content (wt%)

Fig. 2

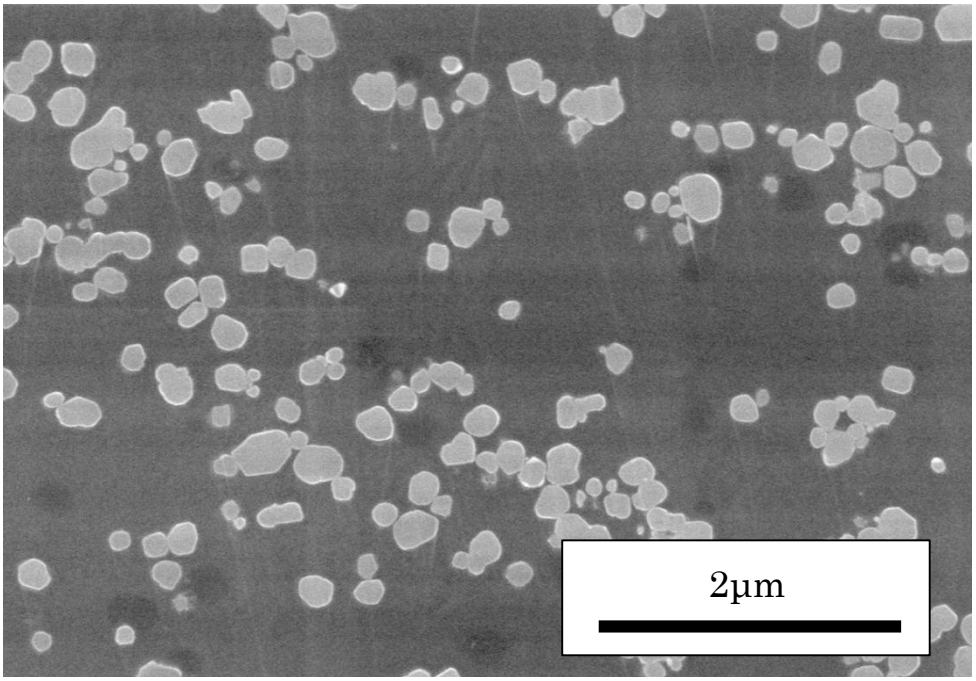

Fig. 3

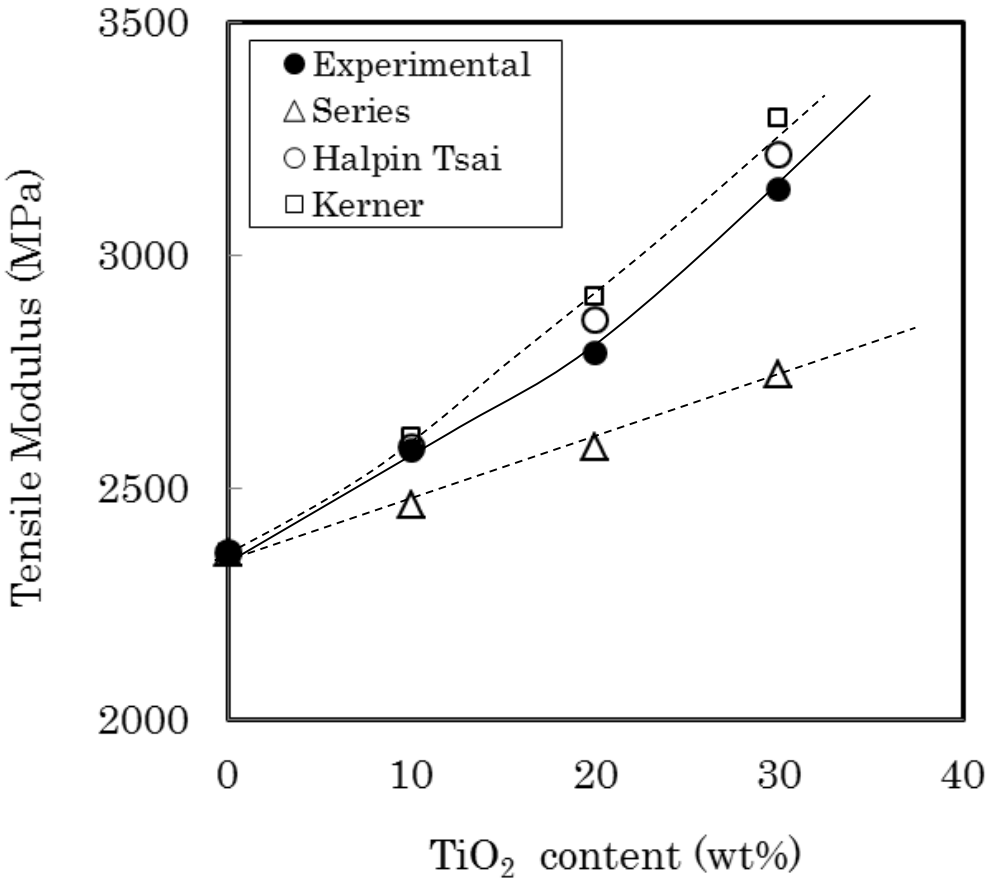
3500
3000
2500
2000
Tensile Modulus (MPa)
Experimental
Series
Halpin Tsai
Kerner
0
10
20
30
40
TiO2 content (wt%)

Fig. 4

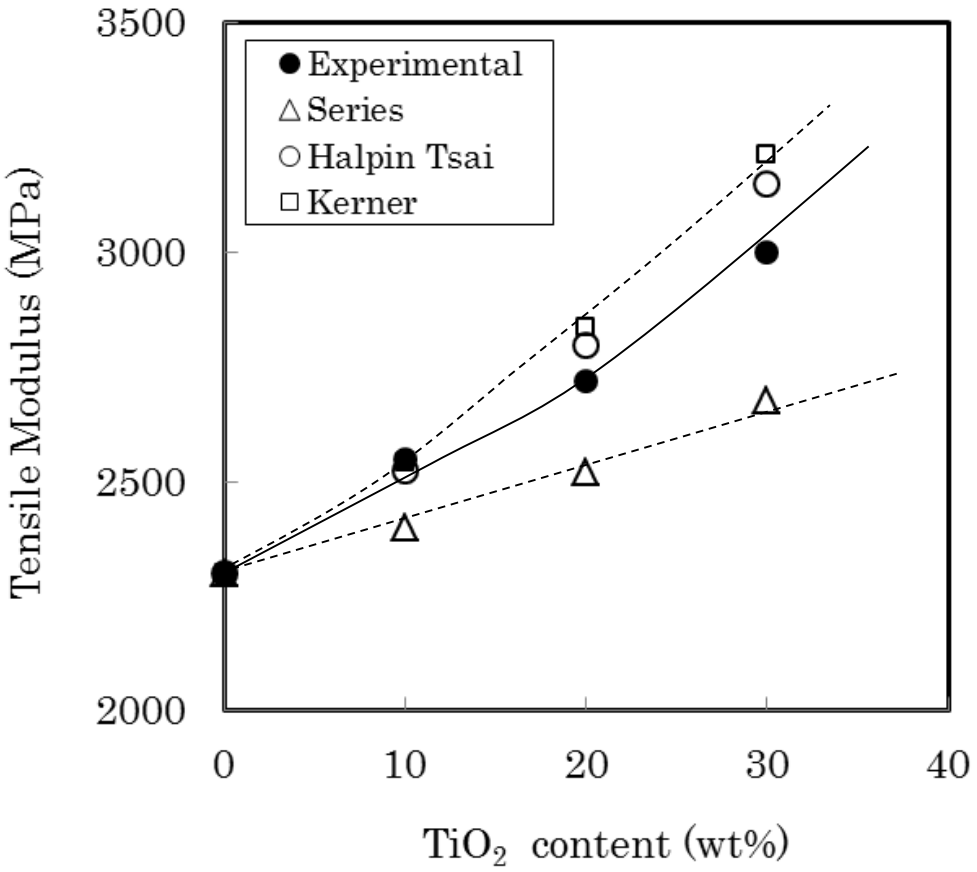
3500
3000
2500
2000
Tensile Modulus (MPa)
Experimental
Series
Halpin Tsai
Kerner
0
10
20
30
40
TiO2 content (wt%)

Fig. 5

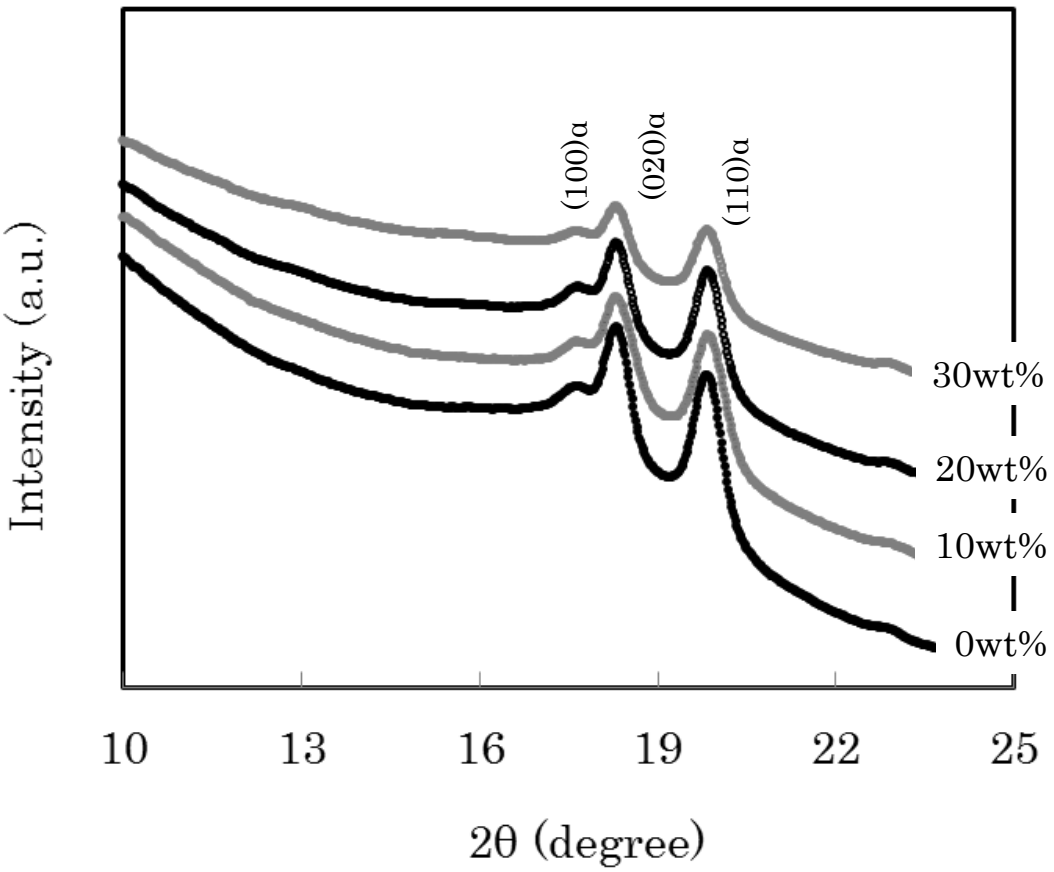
Intensity (a.u.)
(100)α
(020)α
(110)α
30wt%
20wt%
10wt%
0wt%
10
13
16
19
22
25
2θ (degree)

Fig. 6

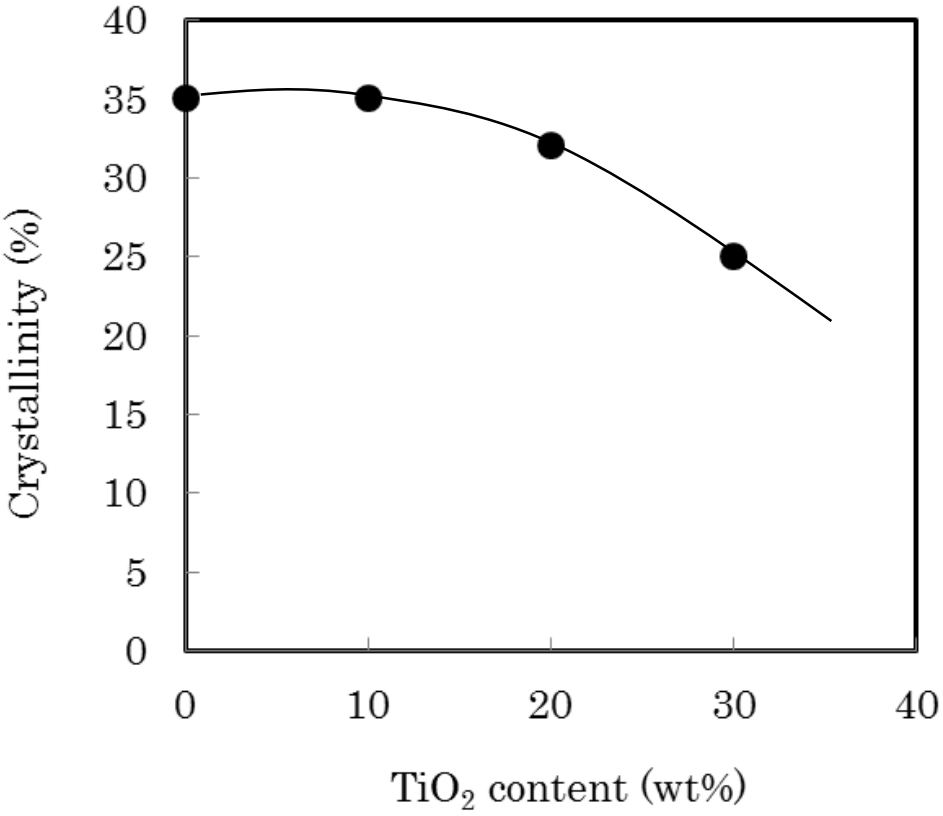
Crystallinity (%)
40
35
30
25
20
15
10
5
0
0
10
20
30
40
TiO2 content (wt%)

Fig. 7

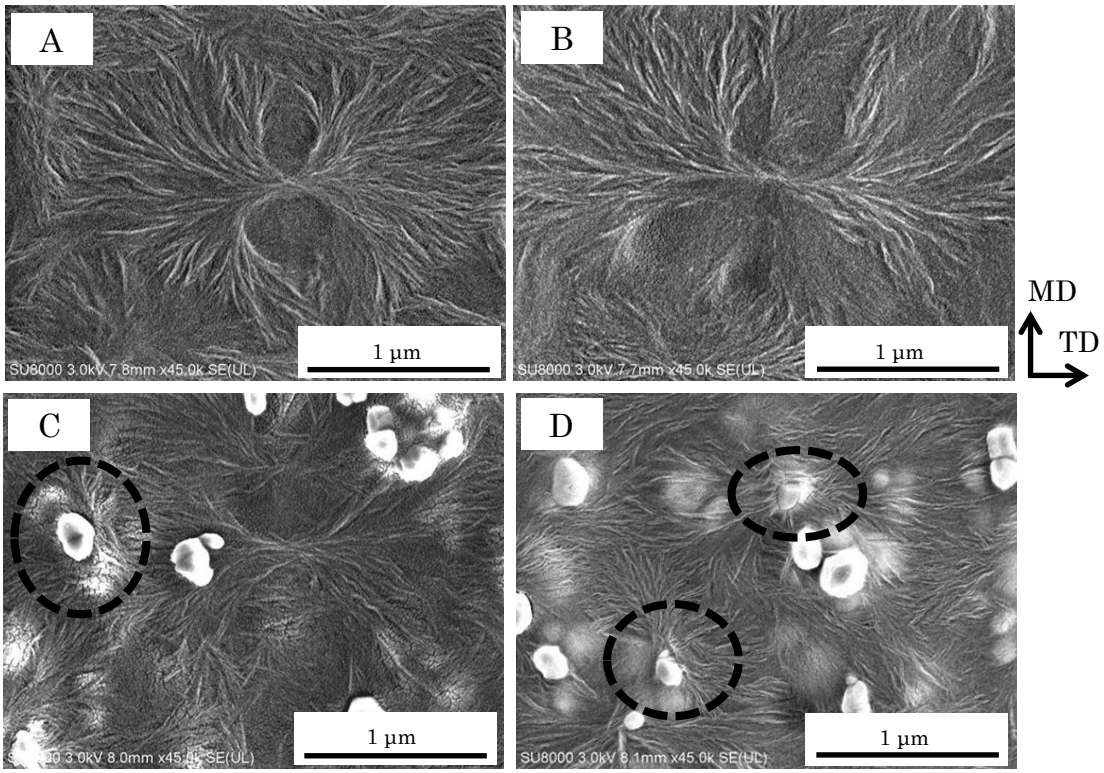

Fig. 8

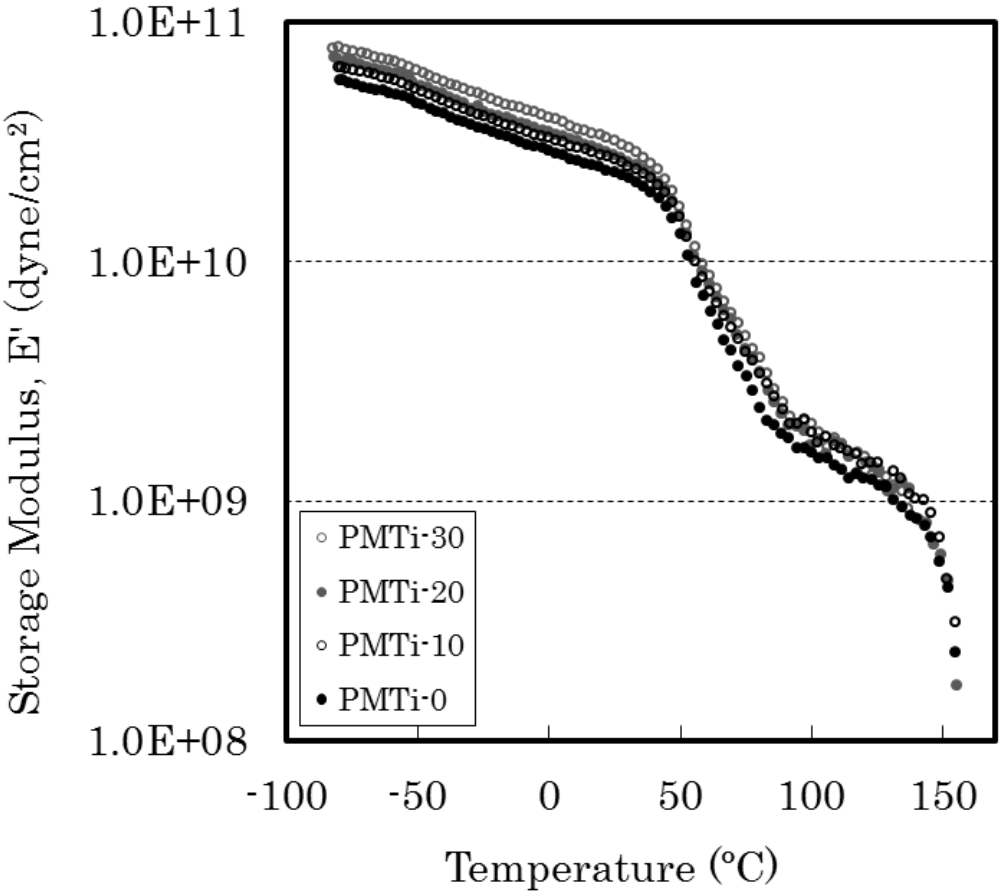
1.0E+11
1.0E+10
1.0E+09
1.0E+08
Storage Modulus, E' (dyne/cm²)
PMTi-30
PMTi-20
PMTi-10
PMTi-0
-100
-50
0
50
100
150
Temperature (°C)

Fig. 9

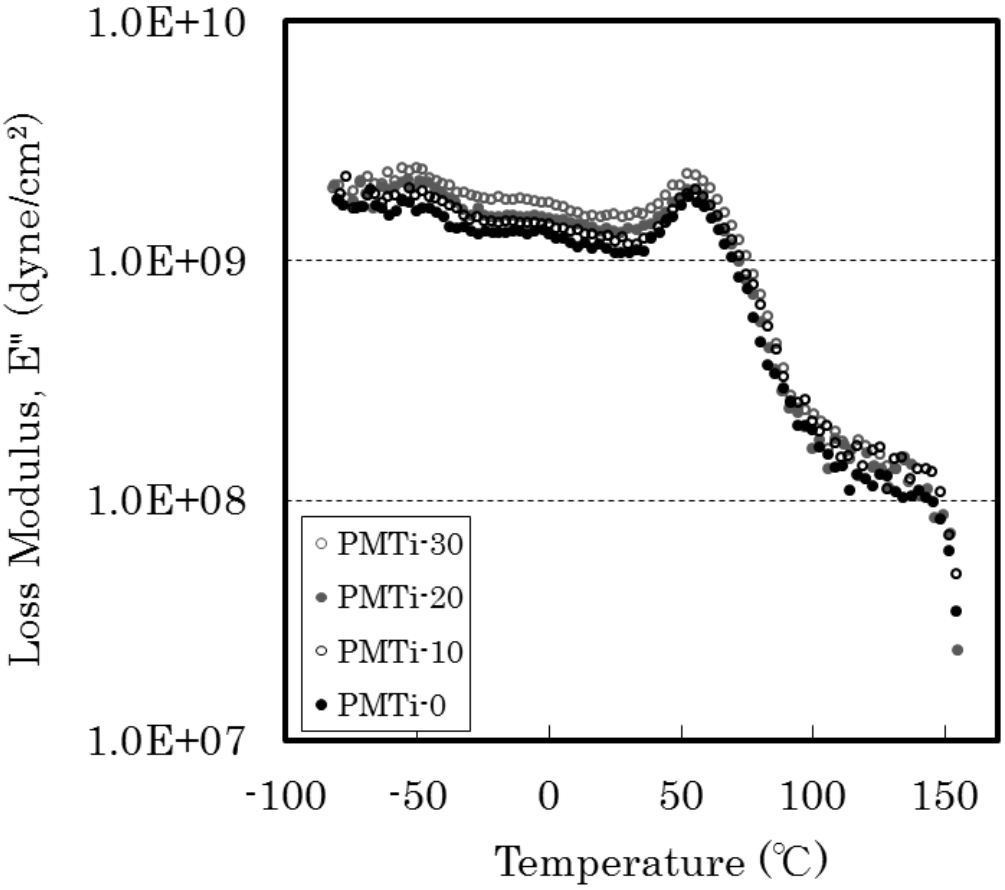
1.0E+10
1.0E+09
1.0E+08
1.0E+07
Loss Modulus, E" (dyne/cm²)
-100
-50
0
50
100
150
Temperature (℃)
PMTi-30
PMTi-20
PMTi-10
PMTi-0

Fig. 10

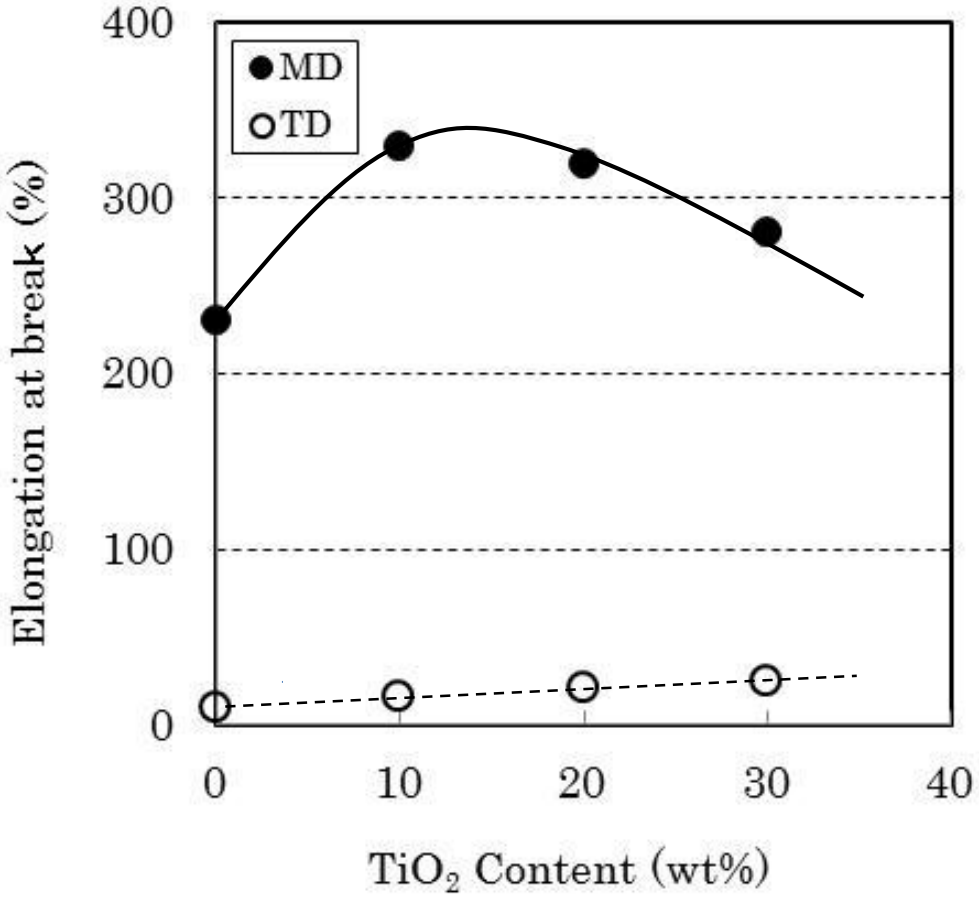
400
300
200
100
0
MD
TD
Elongation at break (%)
0
10
20
30
40
TiO2 Content (wt%)

Fig. 11

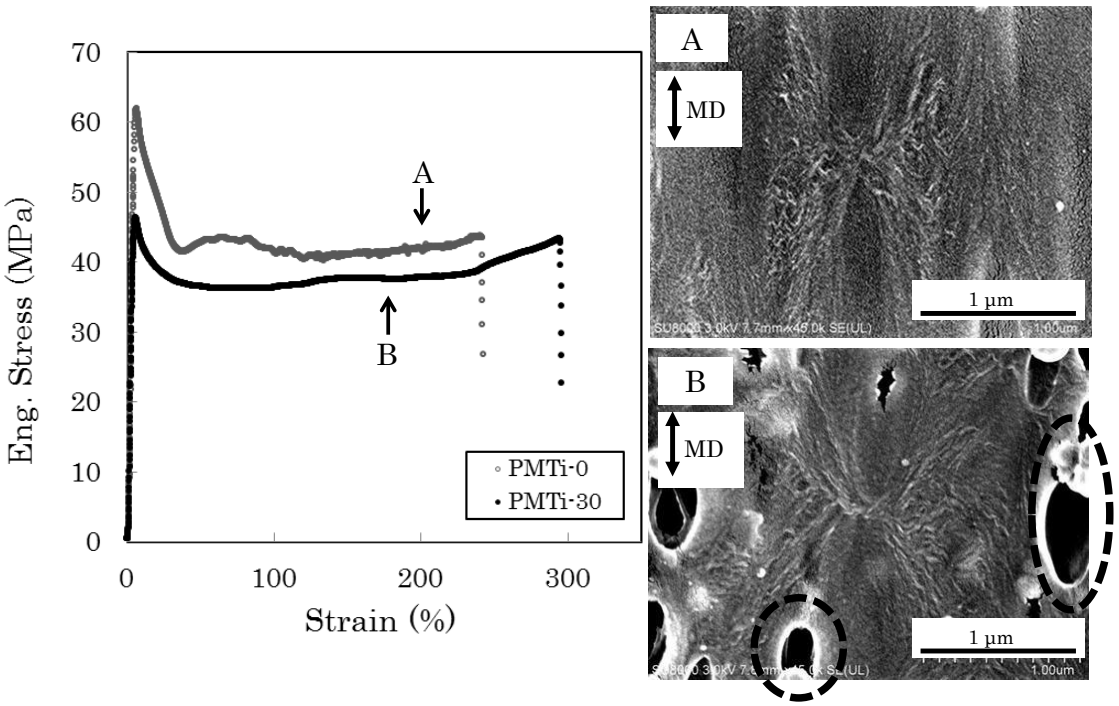
70
60
50
40
30
20
10
0
0
100
200
300
Eng. Stress (MPa)
Strain (%)
A
B
PMTi-0
PMTi-30
A
MD
1 μm
B
MD
1 μm

Fig. 12

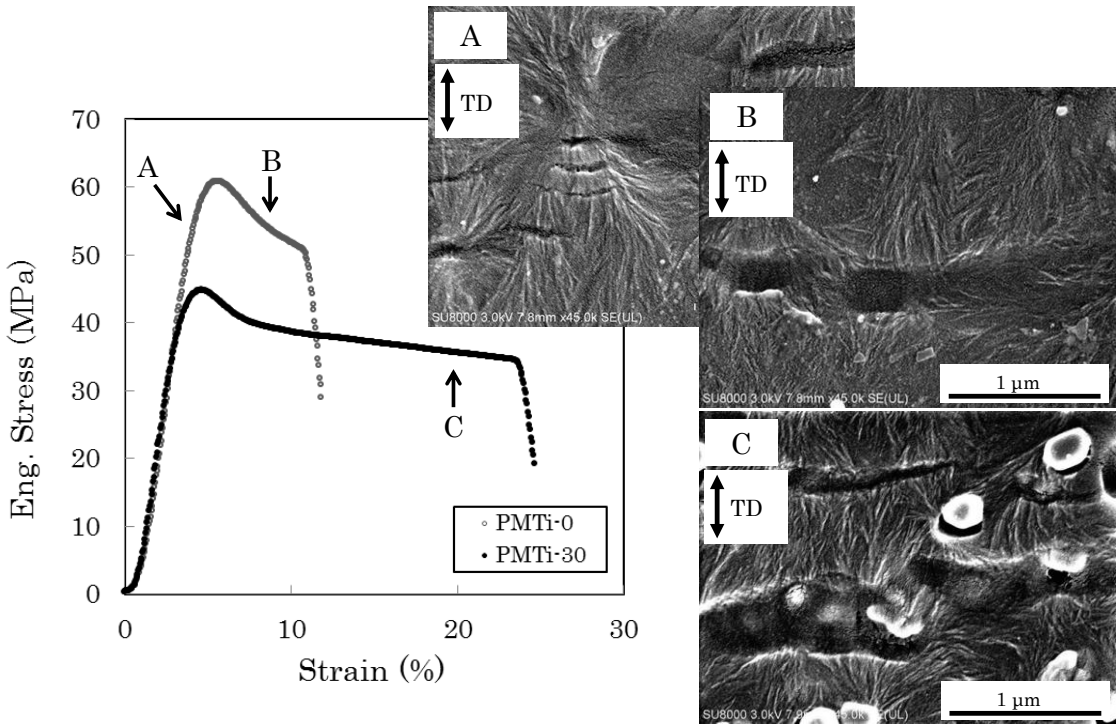
A
TD
B
TD
1 μm
C
TD
1 μm
70
60
50
40
30
20
10
0
0
10
20
30
Eng. Stress (MPa)
Strain (%)
A
B
C
PMTi-0
PMTi-30

Fig. 13

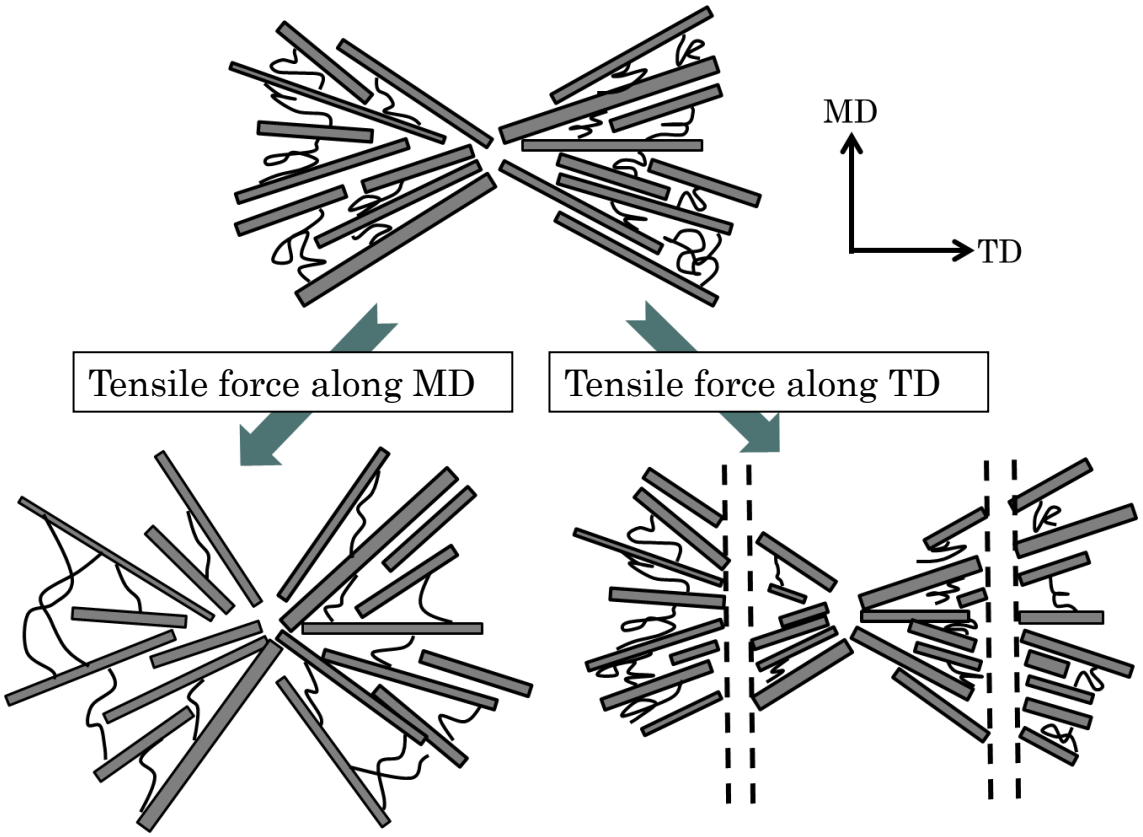

Fig. 14